Cao, T.; Valverde-Muñoz, FJ.; Duan, X.; Zhang, M.; Wang, P.; Xing, L.; Sun, F.... (2021). Spin Crossover in a Series of Non-Hofmann-Type Fe(II) Coordination Polymers Based on [Hg(SeCN)3]-; or [Hg(SeCN)4]2-; Building Blocks. Inorganic Chemistry. 60(15):11048-11057. https://doi.org/10.1021/acs.inorgchem.1c00802

Spin crossover in a series of non-Hofmann type Fe(II) coordination polymers based on $[Hg(SeCN)_3]^-$ or $[Hg(SeCN)_4]^{2-}$ building blocks

Tong Cao,[a,†] Francisco Javier Valverde-Muñoz,[b,†] Xiaoyi Duan,[a] Mingjian Zhang,[a] Ping Wang,[a] Lingbao Xing,[a] Fenggang Sun,[a] Zhen Zhou,[a] Jianzhuang Jiang,[c] M. Carmen Muñoz,[d] José Antonio Real,[b,*] Daopeng Zhang[a,*]

[a]*College of Chemical and Chemical Engineering, Shandong University of Technology, Zibo 255049, PR China. dpzhang73@126.com*

[b]*Instituto de Ciencia Molecular (ICMol), Universitat de València, C/Catedrático José Beltrán Martínez 2, 46980 Paterna (Valencia) Spain. jose.a.real@uv.es.*

[c]*Department of Chemistry, University of Science and Technology Beijing, Beijing 100083, China.*

[d]*Departamento de Física Aplicada, Universitat Politècnica de València, Camino de Vera s/n, E-46022, Valencia, Spain.*

ABSTRACT

Self-assembly of $[Hg(SeCN)_4]^{2-}$ tetrahedral building blocks, ion(II) ions and a series of bis-monodentate pyridyl-type bridging ligands has afforded the new hetero-bimetallic Hg^{II}-Fe^{II} coordination polymers $\{Fe[Hg(SeCN)_3]_2(4,4'\text{-bipy})_2\}_n$ (**1**), $\{Fe[Hg(SeCN)_4](tvp)\}_n$ (**2**), $\{Fe[Hg(SeCN)_3]_2(4,4'\text{-azpy})_2\}_n$ (**3**), $\{Fe[Hg(SeCN)_4](4,4'\text{-azpy})(MeOH)\}_n$ (**4**), $\{Fe[Hg(SeCN)_4](3,3'\text{-bipy})\}_n$ (**5**) and $\{Fe[Hg(SeCN)_4](3,3'\text{-azpy})\}_n$ (**6**), (4,4-bipy = 4,4'-bipyridine, tvp = trans-1,2-bis(4-pyridyl)ethylene, 4,4'-azpy = 4,4'-azobispyridine, 3,3-bipy = 3,3'-bipyridine, 3,3'-azpy = 3,3'-azobispyridine). Single crystal X-ray analyses show that com-

pounds **1** and **3** display a two-dimensional robust sheet structure made up of infinite linear $[(FeL)_n]^{2n+}$ (L = 4,4'-bipy or 4,4'-azpy) chains linked by in situ formed $\{[Hg(L)(SCN)_3]_2\}^{2n-}$ anionic dimeric bridges. Complexes **2** and **4-6** define three-dimensional networks with different topological structures, indicating, in combination with complexes **1** and **3**, that the polarity, length, rigidity and conformation of the bridging organic ligand play an important role in the structural nature of the products here reported. The magnetic properties of complexes **1** and **2** show the occurrence of thermal- and light- induced spin crossover (SCO) properties, while complexes **4-6** are high-spin state at all temperatures. The current results provide a new route for the design and synthesis of new SCO functional materials with non-Hofmann-type traditional structures.

Introduction

Iron(II) spin crossover (SCO) complexes play an important role in chemistry and materials science, not only because they can exhibit magnetic responses to subtle external stimuli, but also because they can provide potential applications as functional materials in data storage and display devices.[1-3] This relevant type of compounds show a rich structural variety ranging from discrete mononuclear and polynuclear oligomers to 1-3D coordination polymers. The Fe^{II} centers usually define hexa-coordinated pseudo-octahedral sites that can be switched between the paramagnetic high-spin (HS) state $t_{2g}^4e_g^2$ (S = 2) and the diamagnetic low-spin $t_{2g}^6e_g^0$ (S = 0) (LS) state in a reversible and controllable way in response to external perturbations, such as temperature, pressure, light irradiation, pulsed magnetic fields, and even by chemical species. Along with the change of spin states, dramatic physical or chemical responses in color, crystal structure, magnetism, optical properties and dielectric constant appear simultaneously, which provides many useful outputs and therefore attracts wide intention from chemist, physicist or material scientist.[4-13]

The use of cyanometallate complexes as bridging ligands has been proven to be a successful strategy for assembling metal ion nodes into a rich diversity of coordination polymers generically known as Hofmann-type compounds. These compounds, discovered more than one century ago,[14,15] were intensively investigated by Iwamoto et al,[16,17] and more recently introduced in the field of SCO by Kitazawa,[18] Real et al.[19,20] Generically formulated $[Fe^{II}(L)_x\{M^{I,II}(CN)_y\}_z]$, SCO Hofmann-type compounds can be structurally classified into two main series: i) 2D layered net-

works with x = 2 and M^{II} = Ni, Pd and Pt (y = 4, z =1) or M^{I} = Cu, Ag, Au (y = 2, z =2) and L is usually a monodentate pyridine-like or triazole-derived ligand; and ii) 3D frameworks with [x = 1, y = 4, z = 1] for M^{II} ions and bismonodentate pyridine-like bridging ligands or [x = 1(2), y = 2, z = 2] for M^{I} ions independently of the bis-monodentate (x = 1) or monodentate (x = 2) nature of the bridging ligand. Most of the advances in this area have been recently reviewed.[21,22]

Obviously, fine tuning and diversity are two important properties featured by the SCO Hofmann-type family, which have been achieved thanks to the use a panoply of organic ligands. However, this strategy is limited by the structural square-planar or linear nature of the cyanometallate building blocks. To go further, an interesting idea that may open new perspectives is to exploit new metalloligand building blocks with different symmetry from the intensely used cyanometallates. In this context, we have introduced in the field of SCO the use of the metalloligand building blocks $K_2[Hg(XCN)_4]$ (X = S, Se) that conveniently combined with Fe^{II} and appropriate bis-monodentate pyridine-like bridging ligands has afforded new SCO compounds with unprecedented non-Hofmann-type 3D coordination polymers $\{Fe(bpe)[Hg(XCN)_4]\}_n$ (bpe = trans-1,2-bis(4-pyridyl)ethane). Similar to the monodentate precursor XCN^- anionic ligands, the ligand-field strength of the tetradentate $[Hg(XCN)_4]^{2-}$ building blocks is larger for X = Se than for X = S. In particular, $\{Fe(bpe)[Hg(SeCN)_4]\}_n$ displays complete thermal- and photo-induced SCO behavior.[23] We also showed previously that the lability of the $[Hg(SCN)_4]^{2-}$ anions could afford a series of novel bimetallic 2D SCO non-Hofmann type coordination polymers $\{Fe(L')[(Hg(SCN)_3)_2]\}n\cdot xSolvent$ (L' = linear bis-monodentate pyridyl ligand). Indeed, the $[Hg(SCN)_4]^{2-}$ ion in presence of suitable bis-monodentate pyridine-like ligands L' in situ transforms into robust dinuclear building units $\{[Hg(SCN)_3]_2(\mu\text{-}L')\}^{2-}$ which determine the formation of the 2D coordination polymers with interesting thermal and photo-induced SCO behavior.[24-26]

Aiming at probing the lability of the $[Hg(SeCN)_4]^{2-}$ bridging ligand and its potential in situ transformation into robust $\{[Hg(SeCN)_3]_2(\mu\text{-}L')\}^{2-}$ building blocks for the synthesis of new SCO coordination polymers, we have investigated the self-assembling of $[Hg(SeCN)_4]^{2-}$, Fe^{II} ion and bis-monodentate pyridine-like ligands with different size, rigidity or coordination topology (Scheme 1). In this respect, here we report the synthesis, crystal structure and magnetic characterization of six new non-Hofmann-like 2D or 3D coordination polymers with different topological structure: $\{Fe[Hg(SeCN)_3]_2(4,4'\text{-bipy})_2\}_n$ (**1**), $\{Fe[Hg(SeCN)_4](tvp)\}_n$ (**2**), $\{Fe[Hg(SeCN)_3]_2(4,4'\text{-azpy})_2\}_n$ (**3**), $\{Fe[Hg(SeCN)_4](4,4'\text{-azpy})(MeOH)\}_n$ (**4**),

{Fe[Hg(SeCN)$_4$](3,3'-bipy)}$_n$ (**5**), {Fe[Hg(SeCN)$_4$](3,3'-azpy)}$_n$ (**6**), (4,4-bipy = 4,4'-bipyridine, tvp = trans-1,2-bis(4-pyridyl)ethylene, 4,4'-azpy = 4,4'-azobispyridine, 3,3-bipy = 3,3'-bipyridine, 3,3'-azpy = 3,3'-azobispyridine). The results show that the structure of these complexes is sensitive to the bridging ligand used. In addition, while compounds **1** and **2** display thermal and photo-induced SCO properties while **4**-**6** are HS complexes. Compound **3** is byproduct in the synthesis of **4** but in contrast to the latter is LS at low temperatures and most probably is also a SCO system.

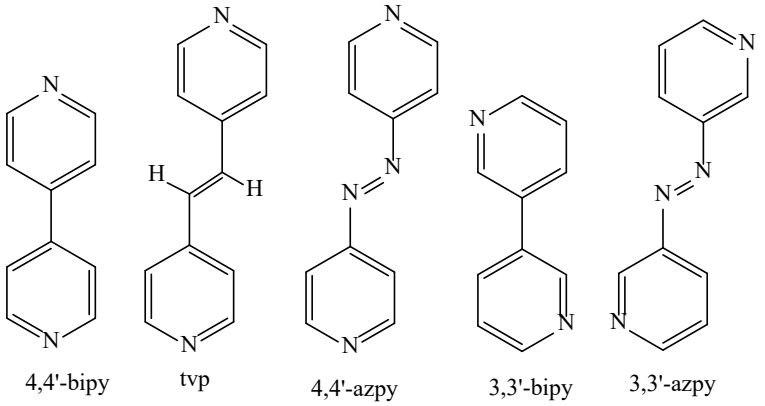

Scheme 1. Ligands used in the present work

Results

Synthesis and general characterization

Slow liquid-liquid diffusion of the three-component system [Fe^{II}/MeOH - $[Hg(SeCN)_4]^{2-}$/H_2O - L/MeOH] has been proved to be an efficient method for assembling them into 2D and 3D coordination polymers (see experimental section). For L = 4,4'-bipy, in situ transformation of the precursor complex $[Hg(SeCN)_4]^{2-}$ into $\{[Hg(SCN)_3]_2(\mu\text{-}L)\}^{2-}$ occurs similarly as previously reported for its X = S counterpart, thereby giving the corresponding isostructural 2D complex **1**. The same in situ transformation also occurs for L = 4,4'-azpy, but in a very small extent, therefore giving a minority product (complex **3**), which has a similar structure to that for complex **1**. It should be pointed out that further characterization on this complex was precluded due to its extremely low yield. Apparently, the equilibrium mostly favors the $[Hg(SeCN)_4]^{2-}$ species as the majority giving compound **4**, which affords a singular 3D CP where the $[Hg(SeCN)_4]^{2-}$ building blocks remain intact but act as three-connecting nodes and one molecule of methanol completes the Fe^{II} octahedron (vide infra). However, the structurally close related ligand L = tvp, produces

exclusively the 3D CP where the $[Hg(SeCN)_4]^{2-}$ centers act as tetra-connecting nodes similarly to the previously reported bpe derivative (bpe (trans-1,2-bis(4-pyridyl)ethane).[23] These results confirm that the discrimination between the 2D or 3D CP structures depends on the metrics and probably flexibility of L. Then, with this in mind, we have included, as an additional variable, the influence of the coordination topology of L on the nature of the resulting CP. Thus, by introducing the 3,3'-positioned pyridyl ligands L = 3,3'-bipy and 3,3'-azpy, with possible *cis*- or *trans*- coordination modes, another two 3D non-Hofmann CPs were successfully synthesized using the same diffusion method.

All the complexes except **3** were characterized by IR spectroscopy (Figures S1-S5, Support Information). In the IR spectra of the complexes, the main peaks with strong intensity attributed to the vibration of SCN groups were observed near 2100 and 2060 cm^{-1}, respectively. Elemental chemical analyses are consistent with the structures obtained from single crystal analysis.

Crystal structure of complexes 1 and 3

Compounds **1** (at 100 and 293 K) and **3** (at 119 K) crystallize in the triclinic space group P-1 (Z = 1). Structurally, both complexes belong to the two-dimensional (2D) hetero-bimetallic spin crossover coordination polymers generically formulated $\{Fe^{II}[(Hg^{II}(SCN)_3)_2](L)_x\}\cdot Solv$ previously reported by us and, consequently, will be described together.[24-26] The coordination environment of the metal ions and the stacking of the 2D layers for complex **1** are shown in Figure 1, while for complex **3** are given in Figure S6. Selected bond lengths and the corresponding average angular distortion parameters Σ^{Fe} and Σ^{Hg} defined as the sum of deviations from the ideal octahedron/tetrahedron of the 12 and 6 "cis" bond angles, $\sum_{12}^{i=1} |\theta i - 90°|$ and $\sum_{6}^{i=1} |\theta i - 109.5°|$,

respectively, are listed Table 1. The structures are characterized by the presence of three inversion centers, one lies on the Fe^{II} site while the other two are located at the middle of the two crystallographically unique 4,4'-bipy or 4,4'-azpy ligands, which have practically a planar conformation. The Fe^{II} ion defines a slightly elongated octahedral $[FeN_6]$ node with the equatorial positions occupied by four nitrogen atoms from four $SeCN^-$ groups, while the axial positions are occupied by the N atoms of one of the two independent L ligands (Figure 1 left), which bridge adjacent Fe^{II} centers defining an array of infinite $[Fe(\mu\text{-}L)]_n^{2n+}$ linear chains all running parallel to [001] (see Figure 1 right). Each equatorial $SeCN^-$ linear group, radiating from the Fe centers

along the [100] and [010] directions, also belongs to the in situ generated equivalent dimeric $\{[Hg(SeCN)_3]_2(\mu\text{-}L)\}^{2-}$ anionic units. The dimers counterbalance the charge of the $[Fe(\mu\text{-}L)]_n^{2n+}$ chains and act as bridges between adjacent chains forming a 2D layer lying parallel to the *a*, *c* plane. These layers stack along *b*. The average Fe-N bond lengths <Fe-N> = 1.956 Å for **1** (100K) and 1.965 Å for **3** (119K) are consistent with the LS state. For **1** this value increases by 0.21 Å up to 2.167 Å at 293K, denoting a complete transformation of the LS state into the HS state in agreement with the magnetic data. As expected, the Σ^{Fe} parameter is larger in the HS state, 17.6° (**1**, 293K), and decreases considerably in the LS state, 5.4° (**1**, 100K). For **3** the Σ^{Fe} value is 8.4° at 119K. Favored by the monodentate nature of the ligands involved in these two compounds, the Σ^{Fe} parameter in the LS state is consistent with the quasi regular octahedral geometry of the above compounds. Unfortunately, complex **3** is a minority byproduct that appears during the formation of the majority complex **4** and we only got a few crystals just to analyze its structure in the LS state since they deteriorated rapidly in the HS state.

The centrosymmetric dimeric units $\{[Hg(L)(SeCN)_3]_2\}^{2-}$ are constituted of two tetrahedral $[HgSe_3N]$ coordination sites. Each tetrahedron is completed with three Se atoms of the almost linear selenocyanate groups and the N atom of the second crystallographically unique centrosymmetric L ligand. Two of the three $SeCN^-$ groups in $[Hg(SeCN)_3]\}^-$ act as bis-monodentate bridging ligands coordinating, as mentioned above, the equatorial positions of the Fe sites of consecutive $[Fe(L)]_n^{2n+}$ chains, while the third one acts a terminal ligand, thereby defining infinite layers (Figure 1 middle and Figure S6). The average <Hg-Se> bond lengths are 2.606, 2.592 and 2.591 Å for **1**(100K), **1** (293K) and **3** (119K), respectively, while the corresponding Hg-N(9) bond lengths are 2.411(8), 2.444(11), 2.410(4) Å. The Hg-SeCN bonds are strongly tilted in both complexes with the three Hg-Se-C bond angles are in the interval 101-89°. The Σ^{Hg} parameter in both complexes are 79.52, 77.37° and 65.58°, indicates that the $[HgSe_3N]$ pseudo-tetrahedral environment is strongly distorted and that the spin state has no relevant influence on the coordination geometry of the Hg^{II} ion.

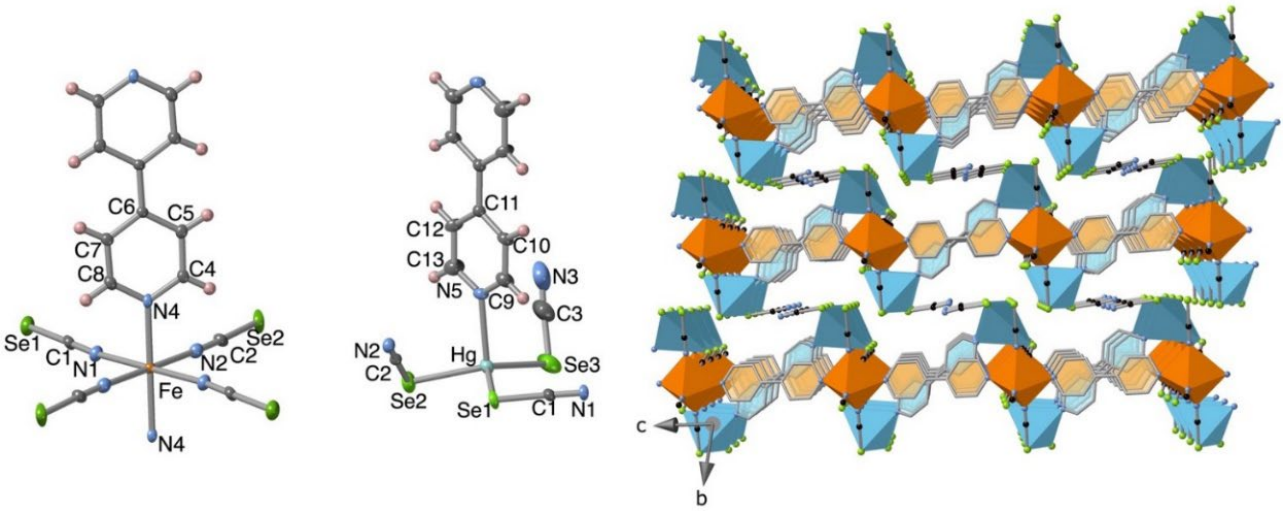

Figure 1. Coordination environment of Fe^{II} (left) and Hg^{II} (middle) for **1**. Stacking of three consecutive layers (right). Colour code: Fe^{II} (orange), Hg^{II} (light blue). The aromatic rings of the 4,4'-bipy ligands defining the infinite $[Fe(\mu\text{-}4,4'\text{-bipy})]_n^{2n+}$ linear chains are filled in orange colour, while those defining the dimeric $\{[Hg(SeCN)_3]_2(\mu\text{-}4,4'\text{-bipy})\}^{2-}$ units are filled in sky blue.

Table 1. Selected bond lengths (Å) and average distortion angles (deg) for complexes **1** and **3.**

Complex **1**	100K	293K	Complex **3** (119K)
Hg(1)-Se(1)	2.6741(10)	2.6513(18)	2.632(2)
Hg(1)-Se(2)	2.5404(11)	2.6035(19)	2.6115(18)
Hg(1)-Se(3)	2.6036(10)	2.522(2)	2.529(2)
Hg(1)-N(9)	2.411(8)	2.444(11)	2.410(4)
Fe(1)-N(1)	1.936(8)	2.153(13)	1.929(13)
Fe(1)-N(2)	1.930(8)	2.160(13)	1.957(13)
Fe(1)-N(4)	2.004(7)	2.188(11)	2.009(13)
Σ^{Fe}	5.4	17.6	8.4
Σ^{Hg}	79.52	77.37	65.58

Crystal structure of complexes 2 and 4

At 293 K and 100 K, **2** adopts the orthorhombic space group Fddd, while **4** shows the mono-clinic space group P21/c at 293 K. Selected bond lengths and angles for complexes **2** and **4** are given in Table 2. Figure 2 displays the coordination environment of the crystallographically unique Fe^{II} and Hg^{II} centers together with the corresponding atom numbering for complexes **2** and **4**. Perspective views of the 3D structures for these two complexes are given in Figure 3.

The Fe^{II} site lies at the center of a slightly distorted [FeN_6] (**2**) or [FeN_5O] (**4**) octahedron whose axial positions are occupied, respectively, by the bridging ligands tvp (**2**) or 4,4'- azpy (**4**) in a similar way. The equatorial positions are occupied by four N atoms (N1 and N2) of four equivalent $[Hg(SeCN)_4]^{2-}$ groups in complex **2**, while three N atoms (N1, N2 and N3) from three equivalent $[Hg(SeCN)_4]^{2-}$ groups and one O atom of a coordinated methanol molecule complete the coordination site in complex **4**. The averaged <Fe-N> value in complex **2** at room temperature, 2.174 Å, is 0.062 Å longer than the corresponding value 2.112 Å at 100 K, thereby indicating that the structure contains a HS:LS mixture of Fe^{II} spin states of ca. 70:30 at this temperature, in perfect agreement with the magnetic measurements (vide infra). The average bond length for the mixed [FeN_5O] coordination center of complex **4** is 2.154 Å. As it will be shown in the description of the magnetic properties, the replacement of a N atom with a more electronegative O atom weakens the ligand field around the Fe^{II} in complex **4** becoming HS at all temperatures. The stabilization of the HS in **4** is also reflected on the angular distortion of the octahedron, Σ^{Fe}, which is markedly larger for **4** (23.5° at 293 K). Interestingly, the OH group belonging to the coordinated methanol molecule defines a strong intramolecular hydrogen bond (d[N4···O1] = 2.741(2) Å and N4···H-O1 = 168.3(1)°) with the uncoordinated terminal N4 atom of the SeCN moiety that does not act as bridge with the Fe center.

At variance with **1** and **3**, the Hg^{II} centers surrounded by four Se donor atoms retain the tetrahedral coordination environment of the starting $[Hg(SeCN)_4]^{2-}$ anion. The angular distortion of the tetrahedron in **2**, Σ^{Hg} = 50° (100 K) and 51.75° (293K) is larger than the corresponding value 34° for **4**, but smaller than the values found for **1** and **3** (see Table 1). The $[Hg(SeCN)_4]^{2-}$ anion acts, respectively, as a tetra- or tri-dentate connecting nodes in complexes **2** and **4** bridging four or three Fe(II) ions along the three mutually perpendicular directions, therefore extending structure into a 3D network (Figure 3). A projection of the networks down the *b* (**2**) and *a* (**4**) directions (Figure 3) allows to describe the structure as made up, in both cases, of layers of Fe^{II} octahedrons laying parallel to *a*-*b* plane separated by layers of tetrahedral anions. In both compounds, the organic and inorganic bridging ligands connect Fe^{II} of consecutive layers.

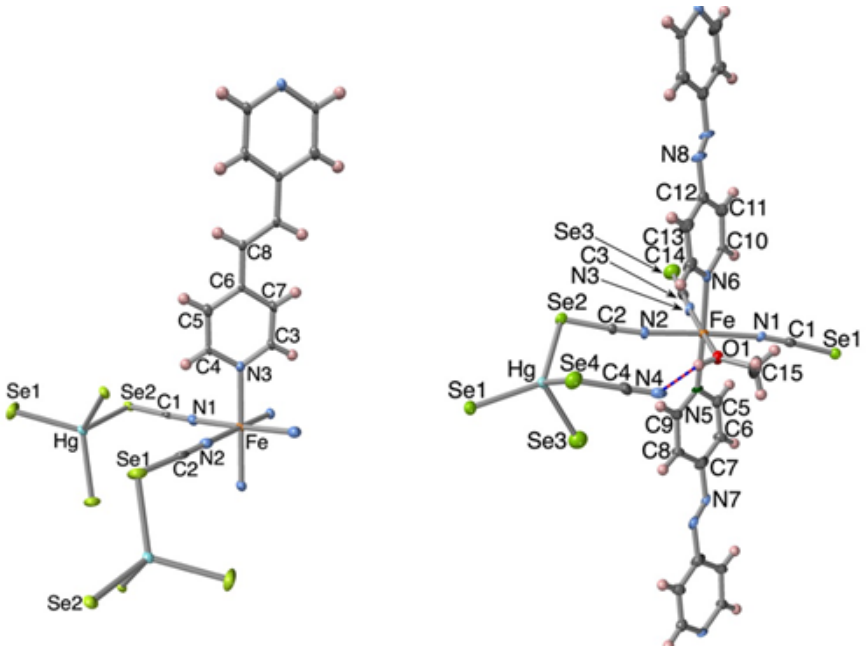

Figure 2. Coordination environment of Fe^{II} and Hg^{II} for compounds **2** (left) and **4** (right).

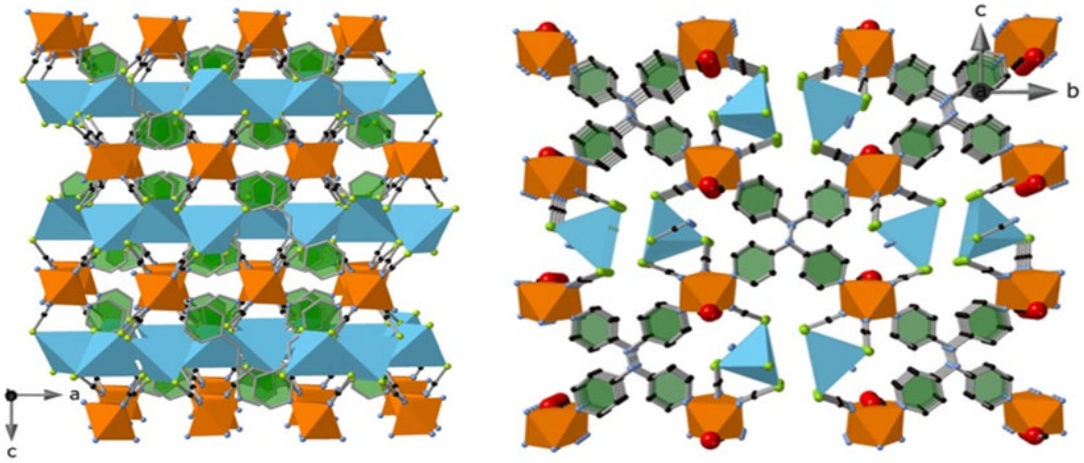

Figure 3. Perspective views of the 3D coordination polymers **2** (top) and **4** (bottom) seen down the *b* and *a* directions, respectively. Color code: Fe^{II} (orange), Hg^{II} (light blue). The aromatic rings of the tvp and 4,4'-azpy ligands are filled in green.

Table 2. Selected bond lengths (Å) and average distortion angles (°) for complexes **2** and **4**.

Complex **2**	293K	100K	Complex **4**	293 K
Hg(1)-Se(1)	2.6854(11)	2.6131(10)	Hg(1)-Se(1)	2.6108(15)
Hg(1)-Se(2)	2.6084(10)	2.6809(10)	Hg(1)-Se(2)	2.6104(14)
Fe(1)-N(1)	2.134(8)	2.079(8)	Hg(1)-Se(3)	2.659(2)
Fe(1)-N(2)	2.170(8)	2.105(8)	Hg(1)-Se(4)	2.6551(18)
Fe(1)-N(3)	2.218(6)	2.153(7)	Fe(1)-N(1)	2.151(12)
Σ^{Fe}	19.2	18.7	Fe(1)-N(2)	2.149(12)
Σ^{Hg}	50	51.75	Fe(1)-N(3)	2.126(11)
			Fe(1)-N(5)	2.203(11)
			Fe(1)-N(6)	2.190(12)
			Fe(1)-O(1)	2.104(8)
			Σ^{Fe}	23.5
			Σ^{Hg}	34.11

Crystal structures of complexes 5 and 6

Both compounds crystallize in the monoclinic space group C2/c and contain four independent units in the unit cell. Figures 4 and 5 show the coordination environment of the metal ions together with the atom numbering and the perspective view of the 3D network while Table 3 gathers the corresponding bond lengths and the average distortions angle of the defined polyhedrons. The Fe^{II} site lies in an inversion center defining a slightly distorted [FeN_6] octahedron with the equatorial positions occupied by four N atoms from four crystallographically identical $[Hg(SeCN)_4]^{2-}$ ions, while the two axial ones are completed by the bridging 3,3-bipy or 3,3'-azpy ligands. The axial <Fe-N> bond lengths are 2.223(7) and 2.200(17) Å for **5** and **6**, respectively, are longer than the averaged equatorial <Fe-N> ones, being 2.141 Å for **5** and 2.142 Å for **6,** indicating the slightly elongated octahedral geometry around the Fe^{II} ion. These bond lengths as well as the Σ^{Fe} values 21.6° (**5**), 15.2° (**6**) are consistent with the HS state of the Fe^{II} ion (vide infra).

The Hg^{II} ions define a triflingly distorted tetrahedron generated by two crystallographically independent selenocyanate groups, for which it can be proved by the bond parameters around and the corresponding Σ^{Hg} values 22.09° and 16.04°. The $[Hg(SeCN)_4]^{2-}$ building block in **5** and **6** acting tetradentate ligand links four Fe^{II} ions by using its two pairs of the $SeCN^-$ groups along the

almost orthogonal directions, therefore extending the zig-zag or wave-like chains into three-dimensional network (Figure S7). The two SeCN-Fe units in complexes **5** or **6** show a little difference, in which one presents a perfect linear conformation while the other is somewhat bent with the Se-CN-Fe bond angles 153.12(2) and 164.59(3)°, respectively. Additional, it should be pointed out that there exist comparatively strong π-π stacking interactions in complex **5** between the pyridine rings of the 3,3'-bipy ligands with the center-center distance 3.848(2) Å.

Both coordination polymers seen down the *c* axis direction (see Figure 5) can be described as formed by layers of Fe^{II} octahedral sites laying parallel to the *a-c* plane and stacking along *b* direction. The most relevant structural difference between both compounds derives from the different conformation adopted by the bridging ligand when coordinates two consecutive Fe^{II} centers, namely the 3,3'-bipy ligand (compound **5)** adopts a *cis* conformation with respect to the two coordinating N atoms while the ligand 3,3'-azpy adopts a *trans* conformation (compound **6**) (Figure S7). Consequently, the 3,3'-bipy ligand connects two consecutive Fe^{II} centers belonging to the same layer while, in contrast, the 3,3'-azpy ligand links the Fe^{II} centers of two consecutive layers. Another relevant consequence is that the tetrahedral $[Hg(SeCN)_4]^{2-}$ centers, are differently located in both structures. They are placed between the layers, connecting the Fe^{II} centers of two adjacent layers, for the 3,3'-bipy derivative, while they are placed within the same layer connecting consecutive Fe^{II} centers of the same layer for the 3,3'-azpy derivative. Obviously, the distinct topologies adopted by both network compounds are correlated with the different flexibility and/or size of the organic bridging ligands.

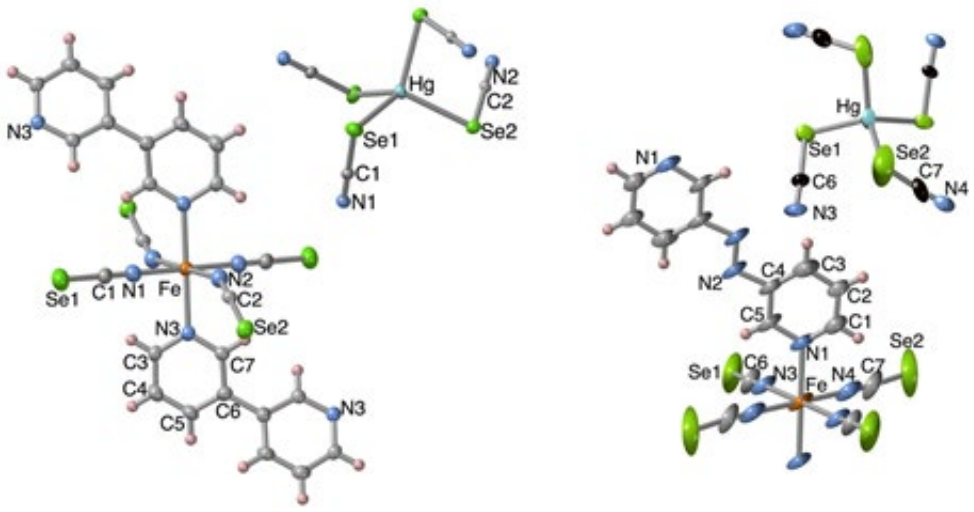

Figure 4. Coordination environment of Fe^{II} and Hg^{II} for compounds **5** (left) and **6** (right).

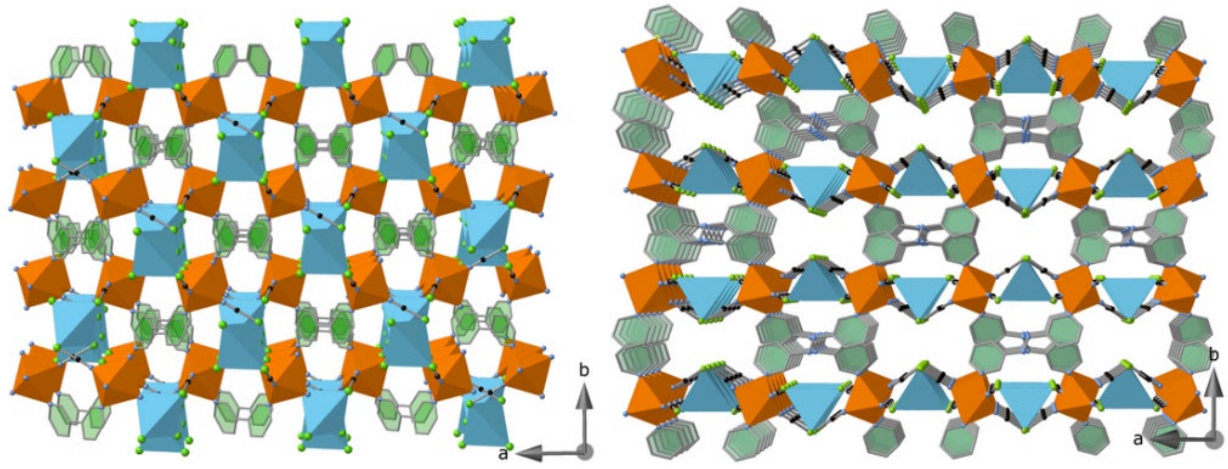

Figure 5. Perspective views down the c direction for the 3D nets **5** (top) and **6** (down) showing the bridging *cis* and *trans* conformations adopted by the 3,3'-bipy and 3,3'-azpy ligands, respectively. Color code: Fe^{II} (orange), Hg^{II} (light blue). The aromatic rings of the 3,3'-bipy and 3,3'-azpy ligands are filled in green.

Table 3. Selected bond lengths (Å) and average distortion angles (°) for complexes **5** and **6**.

Complex **5**		Complex **6**	
Hg(1)-Se(1)	2.6541(10)	Hg(1)-Se(1)	2.599(5)
Hg(1)-Se(2)	2.6553(10)	Hg(1)-Se(2)	2.662(8)
Fe(1)-N(1)	2.130(7)	Fe(1)-N(1)	2.200(17)
Fe(1)-N(2)	2.153(8)	Fe(1)-N(3)	2.154(15)
Fe(1)-N(3)	2.223(7)	Fe(1)-N(4)	2.13(4)
Se(1)-C(1)	1.806(9)	Se(1)-C(6)	1.78(2)
Se(1)-C(2)	1.805(9)	Se(1)-C(7)	1.79(5)
Σ^{Hg}	22.99	Σ^{Hg}	16.04
Σ^{Fe}	21.6	Σ^{Fe}	15.2

Magnetic properties of complexes 1-6

Temperature dependent magnetic susceptibility measurements have been carried out for all the complexes (except **3**) in the temperature interval 10-300 K under an external magnetic field of 1000 Oe by using samples constituted of 10-20 mg single crystals. The thermal dependence of the $\chi_m T$ product (χ_m = magnetic susceptibility, T = temperature) for complexes **1** and **2** are shown in Figure 6, and those for other complexes **4-6** are given in Figures S8-S10, respectively.

At room temperature, the $\chi_m T$ are about 3.6 and 3.8 cm^3 K mol^{-1} for complexes **1** and **2**, respectively, a value consistent with the Fe^{II} ion in the HS (S = 2) state. For complex **1**, $\chi_m T$ re-

mains practically constant upon cooling to ca. 230 K. Then, $\chi_m T$ drops, reaching a value of 0.1 cm^3 K mol^{-1} at 135 K consistent with the Fe^{II} ion in the LS (S = 0) state. This behavior corresponds well to a complete HS ↔ LS spin transition characterized by the equilibrium temperature $T_{1/2}$ = 166 K, the point of the HS and LS molar fractions equal to 0.5. $\chi_m T$ vs T plots in the cooling and heating modes match perfectly, indicating the absence of thermal hysteresis. Complex **2** also undergoes a spin transition but shifted to lower temperatures than that observed for **1**. Indeed, $\chi_m T$ remains constant upon cooling down to 150 K and then gradually decreases to achieve a minimum of 1.80 cm^3 K mol^{-1} at ca. 70 K, a value which is consistent with a 50 % of HS to LS conversion. This extent of transformation is in reasonable agreement with the average Fe-N bond length mentioned above. It is worth stressing that the large plateau defining the incompleteness of the spin transition occurs at temperatures below 100 K where the kinetics of the HS ↔LS equilibrium becomes very slow remaining "frozen" practically 50% of the HS centers. A $T_{1/2}$ value of ca. 100 K is a reasonable eye estimation for the complete SCO, which is close to that found for the homologous $\{Fe(bpe)[Hg(SeCN)_4]\}_n$. [23]

In order to estimate the thermodynamic parameters associated with the SCO behavior in **1** and **2** the spin transition was simulated using the mean-field regular solution model described by eqn. (1):[25] (Figure S11)

$$ln\left[\frac{1-\gamma_{HS}}{\gamma_{HS}-\gamma_{HS}^{R}}\right] = \frac{\Delta H + \Gamma\,(1+\gamma_{HS}^{R}-2\gamma_{HS})}{RT} - \frac{\Delta S}{R}, \qquad (1)$$

where ΔH and ΔS are respectively the enthalpy and the entropy variations at the transition, while Γ is the interaction parameter accounting for the cooperative nature of the spin conversion, respectively. Here, γ_{HS}^{R} accounts for the residual HS fraction at low-temperature. The HS molar fraction, γ_{HS}, is obtained from the magnetic susceptibility through eqn. (2):

$$\gamma_{HS} = [(\chi_M T)-(\chi_M T)_{LS}]/[(\chi_M T)_{HS}-(\chi_M T)_{LS}], \qquad (2)$$

and the remaining HS molar fraction γ_{HS}^{R} blocked at low temperatures through eqn. (3):

$$(\gamma_{HS})^{R} = (\chi_M T)^{R}/(\chi_M T)^{HS}, \qquad (3)$$

where, $(\chi_M T)$, $(\chi_M T)^{HS}$, $(\chi_M T)^{LS}$ and $(\chi_M T)^{R}$ are the $\chi_M T$ values at any temperature, of the pure HS state ($T\rightarrow\infty$) , of the pure LS ($(\chi_M T)^{LS} \approx 0$) and of the residual species blocked at low temperature in the HS state. Furthermore, taking into account that $T_{1/2}$ (temperature at which γ_{HS} =

γ_{LS} = 0.5, i.e. $\Delta G = 0$), ΔH and ΔS are related through $T_{1/2} = \Delta H/\Delta S$, we have substituted ΔH with ($T_{1/2}\cdot\Delta S$) in eqn (1). Reasonable good simulation curves afford: $T_{1/2}$ = 171 (**1**), 107 (**2**) K; Γ = 1.5 (**1**), 0.4 (**2**) kJ/mol; $(\chi_M T)^{HS}$ = 3.62 (**1**), 3.85 (**2**) cm^3 K/mol; $(\chi_M T)^{R}$ = 0.0 (**1**), 1.77 (**2**) cm^3 K/mol; ΔS = 78 (**1**), 40 (**2**) J/Kmol; and ΔH = 13.3 (**1**), 4.3 (**2**) kJ/mol. These values are consistent with ones obtained for the related coordination polymers $\{Fe(bpe)[Hg(XCN)_4]\}n$[23] and $\{Fe^{II}[(Hg^{II}(SCN)_3)_2](tvp)_2\}$.[25]

Photogeneration of the metastable HS* state at low temperature, namely the light-induced excited spin state trapping (LIESST) experiment, was carried out on microcrystalline samples (about 2-3 mg) of complexes **1** and **2**. Both complexes show traceable photo-induced spin transition (Figure 6). The sample of complexes **1** (**2**) were slowly cooled to 10 K, where $\chi_m T \approx 0.01$ (1.70) cm^3 K mol^{-1}, and then they were irradiated with red light (λ = 633 nm) reaching rapidly (less than half an hour) a $\chi_m T$ saturation value of ca. 3.01 (3.51) cm^3 K mol^{-1}. Afterwards, light irradiation was switched off and the temperature was increased at a rate of 0.3 K min^{-1}. Within the temperature range of 10-40 K, $\chi_m T$ increases up to a maximum value of ca. 3.53 cm^3 K mol^{-1} at 40 K for **1**, reflecting the thermal population of the microstates arising from the zero-field splitting (ZFS) characteristic of the HS* (S = 2) state, and suggests that the light-induced population of this state is rather complete at 10 K. At temperatures higher than 40 K, $\chi_m T$ drops rapidly, attaining a value of about 0.01 cm^3 K mol^{-1} at ca. 60 K, which indicates a practically complete HS* → LS relaxation. For **2**, the increase of $\chi_m T$ in the dark is much limited, due probably to a much lower value of the zero-field splitting characteristic of the S = 2 state, and attains a value of ca. 3.70 cm^3 K mol^{-1} at about 20 K remaining constant up to ca. 50 K, then $\chi_m T$ decreases rapidly to reach a value of ca. 1.80 cm^3 K mol^{-1} at 77 K. The T_{LIESST} value determined from $\partial\chi_m T/\partial T$ in the HS → LS relaxation is 45 K and 68 K for **1** and **2**, respectively. These values are consistent with the empirical inverse energy-gap law,[27-30] i.e. the metastability of the photo-generated HS* species decreases as the stability of the LS increases ($T_{1/2}$ increases). These T_{LIESST} temperatures are perfectly consistent with the correlation line $T_{LIESST} = T_0 - 0.3T_{1/2}$ for which a T_0 value equal to 100 K has been associated with quite regular $[FeN_6]$ coordination environments generated by ligands with small geometrical constraints, as it is the present case.[31] The T_0 value found for **2** is virtually the same as found for the compound $\{Fe(bpe)[Hg(SeCN)_4]\}_n$ mentioned above.[23]

Due to the extremely low yield of complex **3**, we could only study its structure at 119 K which shows that the compound is in the LS state at this temperature. Although this derivative can fore-

seeably present SCO behavior, we were unable to measure neither the thermal dependence of its magnetic properties or its structure at room temperature to confirm it. The remaining complexes **4**-**6** show $\chi_m T$ values within a narrow range, 3.54-3.60 cm^3 K mol^{-1}, that keep almost constant down to about 50K, indicating the typical HS state of the Fe^{II} ion in these complexes. Below 50 K $\chi_m T$ decreases for complexes **4** and **6** down to about 2.7 cm3 K mol−1 at 2K indicating the occurrence of zero-field splitting (ZFS) characteristic of the S = 2 state. Interestingly, complex **5** show a more marked decrease until 1.73 cm^3 K mol^{-1}. The further obvious decreasing of $\chi_m T$ for **5** in the low temperature range implies maybe the weak antiferromagnetic coupling in addition to ZFS between the adjacent high spin Fe^{II} ions. The χm^{-1} versus T curve can be satisfied fitted by Curie-Weiss law within 10-300K, leading to negative Weiss constant. As described in the crystal structure section, the obvious inter-chain π-π stack interaction can be found between the pyridine rings in complex **5**, which can usually result in intermolecular antiferromagnetic interaction and therefore can be used to support the above discussed magnetism phenomenon in this complex.

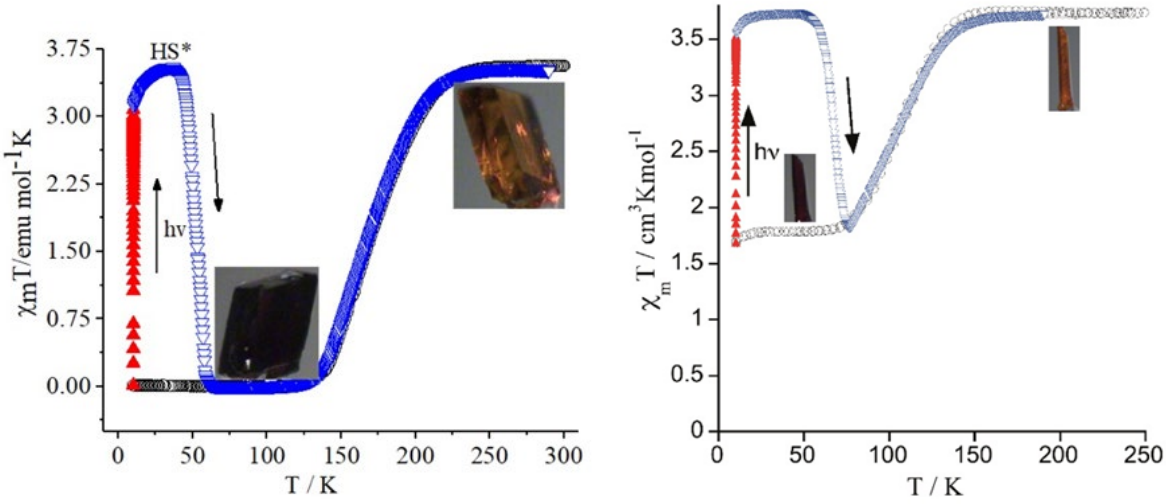

Figure 6. Magnetic properties of complex **1**(left) and **2**(right).

Discussion and Concluding Remarks

Self-assembling $[Hg(SeCN)_4]^{2-}$, Fe^{II} and L rodlike bis-monodentate pyridine-like ligands has afforded a new series of six non-Hofmann type heterobimetallic coordination polymers, which have been structurally characterized and magnetically investigated.

Single crystal X-ray diffraction analysis reveals that when L is 4,4'-bipy or 4,4'-azpy (complexes **1** and **3**), in situ generation of $\{[Hg^{II}(SeCN)_3]_2(\mu\text{-}L)\}^{2-}$ (L = bridge ligand)

dinuclear species are favored. In addition, these dinuclear species in turn act as linkers between linear $[Fe(\mu\text{-}L)]_n^{2n+}$ chains, thus resulting in highly crystalline 2D sheet-like coordination polymers generically formulated $\{Fe[\mu\text{-}(Hg(XCN)_3)_2](\mu\text{-}L)_2\}$ (X = S, Se). Both compounds are isostructural to those obtained from the homologous $[Hg(SCN)_4]^{2-}$ precursor when using equivalent L bis-monodentate ligands, including among others 4,4'-bipy[24,25] or tvp[26]. Based on the limited number of examples reported so far, this in situ transformation from $[Hg(XCN)_4]^{2-}$ to $\{[Hg^{II}(XCN)_3]_2(\mu\text{-}L)\}^{2-}$ seems to be much less favored for X = Se. Indeed, the ligand 4,4'-azpy marginally forms the 2D system (compound **3**) giving essentially the 3D coordination polymer where the $[Hg(SeCN)_4]^{2-}$ building blocks remain intact (compound **4**). Similarly, the ligand tvp gives 100% of 3D species (compound **2**), a fact that strongly contrasts when using $[Hg(SCN)_4]^{2-}$ as starting material, since the latter affords exclusively the 2D compound.[26] The main difference between **2** and **4** is that, unexpectedly, the Fe^{II} centers of the latter retains coordinated a CH_3OH molecule, which interacts via hydrogen bonding with the N atom of the terminal $NCSe^-$ group. In contrast, the ligand 4,4'-bipy favors the transformation of the starting $[Hg(XCN)_4]^{2-}$ species whatever X (S or Se). Possibly, the smaller length and flexibility of 4,4'-bipy together with the imposed coordination topology (lineal) are structural obstacles preventing the accomplishment of the metrics imposed by the $[Hg(XCN)_4]^{2-}$ building blocks to give the 3D compound. However, the opposite is true for its 3,3'-bipy isomer in compound **5**. The "cis-gauche" conformation adopted by the 3,3'-bipy ligand is likely the only structural compromise compatible with the $[Hg(XCN)_4]^{2-}$ building blocks. This conjecture seems to be supported by the fact that the longer 3,3'-azpy in compound **6** adopts an "trans-anti" configuration similarly to the tvp derivative **2**.

Complexes **1** and **2** show temperature and light induced SCO behavior. In contrast to its isostructural X = S homologue that shows a three-step SCO behavior between the states [HS]↔[HS:LS]↔ [HS:2LS]↔[LS], the complete SCO of **1** takes place in only one step between the fully HS and LS states, a fact denoting that the occurrence of multi-step SCO behavior depends on subtle structural differences. Furthermore, the equilibrium temperature for **1**, $T_{1/2}$ = 170 K, is 55 K higher than the average $T_{1/2}$ shown by its X = S homologue.[24,25] This suggests that the increase of ligand field strength around the Fe^{II} induced by the XCN^- (X = S, Se) group does not depend substantially on whether it belongs

to the dimeric bridging unit $\{[Hg^{II}(XCN)_3]_2(\mu\text{-}L)\}^{2-}$ or acts as a simple coordinating terminal anion. It is worth noting that differences of similar magnitude in $T_{1/2}$ have been found for monomeric[35-44] and polymeric 1D[45-47] and 2D[48-51] $[Fe(L)_2(NCX)_2]$ SCO complexes. Interestingly, from a point of view of the coordination sphere of the Fe^{II} ion, the latter series of compounds represent the antithesis of the compounds here described. For example, in the 2D polymers $[Fe(L)_2(NCX)_2]$ (X = S, Se), the equatorial positions of the hexa-coordinated Fe^{II} ion are occupied by four organic bridging ligands L and the axial positions are filled with the two pseudohalide XCN^- anions while the opposite situation is adopted in $\{Fe[\mu\text{-}(Hg(XCN)_3)_2](\mu\text{-}L)_2\}$.

As far as complex **2** is concerned, only ca. 50% of the Fe^{II} centers transform from the HS to the LS state with a characteristic temperature $T_{1/2} \approx 100$ K. The low temperatures at which this SCO occurs points to a kinetic blocking of the remaining 50% HS species since usually below 100 K the dynamics of the SCO of the HS-LS transformation slows down dramatically. This result is consistent with the complete SCO behavior ($T_{1/2}$ = 107.8 K) observed for the isostructural {Fe(bpe)[Hg(SeCN)$_4$]} derivative, where bpe (trans-1,2-bis(4-pyridyl)ethane) is the aliphatic version of the tvp. Furthermore, it confirms that the ligand field felt by the Fe^{II} centers in these 3D compounds is weaker than that observed for the 2D $\{Fe[Hg(SeCN)_3]_2(L)_2\}_n$ series despite the Fe^{II} centers show the same coordination environment.

The lack of SCO in compounds **5** and **6** despite displaying similar 3D structures and $[FeN_6]$ octahedral environment than **2** may be due to a slightly smaller σ-donor capability of the bridging 3,3'-bipy and 3,3'-azpy ligands with respect to bpe or tvp. This is tentatively supported by the fact that the 2D compounds $[Fe(3,3'\text{-bipy})_2(NCX)_2]\cdot 2CHCl_3$ (X = S, Se) are fully HS at any temperature,[52] while both 2D homologous $[Fe(4,4'\text{-bipy})_2(NCX)_2]\cdot 4CHCl_3$ (X = S, Se) display SCO.[51]

New examples with both new structural types and potential interesting SCO behavior based-on $[Hg(XCN)_4]^{2-}$ (X = S, Se) metallo anion ligands as suitable building blocks and other undeveloped mono- or multi-dentate bridging linkers for generating non-Hofmann type topologic structures are undergoing in our lab.

Experimental

Physical methods and materials.

All operations were carried out at room temperature under an air atmosphere and all chemicals and solvents were of reagent grade and used without further purification. 4,4'-Bipyridine, $FeCl_2$, KSeCN, $Hg(SeCN)_2$, trans-1,2-bis(4-pyridyl)ethylene (tvp) were purchased from commercial sources. 4,4'-Azobispyridine (4,4'-azpy), 3,3'-Azobispyridine(3,3-azpy) and 3,3'-bipyridine were prepared following the literature method.[32,33]

Preparation of complexes 1-6.

The six complexes were obtained by diffusion method in three-arms H-type vessels. One arm of the vessel contained a methanol solution (1 mL) of $FeCl_2$ (0.10 mmol, 12.7 mg) and a small amount of crystals of ascorbic acid to avoid oxidation of Fe^{II}, while the middle arm contained a water solution of $K_2[Hg(SeCN)_4]$ (1 mL) prepared in situ by mixing $Hg(SeCN)_2$ (0.1 mmol, 41 mg) and KSeCN (0.2 mmol, 28.8mg). A methanol solution (1 mL) of L (0.10 mmol, L = 3,3'-azpy, 18.4 mg; tvp, 18.2 mg; 3,3'-bipy, 15.6 mg; 4,4'-azpy, 18.4 mg, 4,4-bipy, 15.6 mg) was added to the third arm. After slowly adding methanol to completely fill the three arms, the vessels were sealed, and kept in a quiet and dark place. The crystals of all the complexes except **3** suitable for single crystal X-ray analysis were obtained after about 2-3 weeks with the yield about 50-60%.

Complex **1**: Anal. Calcd. For $C_{26}H_{16}FeHg_2N_{10}Se_6$ (**1**): C, 22.32; H, 1.15; N, 10.01; Found: C, 22.21; H, 1.24; N, 10.09. Main IR bands (cm^{-1}): 2100, 2060 (s, ν_{SeCN}).

Complex **2**: Anal. Calcd. For $C_{16}H_{10}FeHgN_6Se_4$ (**2**): C, 22.38; H, 1.17; N, 9.79; Found: C, 22.28; H, 1.26; N, 9.90. Main IR bands (cm^{-1}): 2100 (s, ν_{SeCN}).

Complex **3**: This complex was a byproduct and crystallized simultaneously with complex **4**. Very few small crystals suitable for X-ray diffraction but with different morphologies from the main component was picked out manually.

Complex **4**: Anal. Calcd. For $C_{15}H_{12}FeHgN_8OSe_4$ (**4**): C, 20.18; H, 1.36; N, 12.55; Found: C, 20.29; H, 1.28; N, 12.65. Main IR bands (cm^{-1}): 2100, 2055 (s, ν_{SeCN}).

Complex **5**: Anal. Calcd. For $C_{14}H_8FeHgN_6Se_4$ (**5**): C, 20.20; H, 0.97; N, 10.10; Found: C, 20.31; H, 1.05; N, 10.19. Main IR bands (cm^{-1}): 2100, 2060 (s, ν_{SeCN}).

Complex **6**: Anal. Calcd. For $C_{14}H_8FeHgN_8Se_4$ (**6**): C, 19.54; H, 0.94; N, 13.02; Found: C, 19.66; H, 1.04; N, 12.90. Main IR bands (cm^{-1}): 2110, 2065 (s, ν_{SeCN}).

Physical Measurements.

C, H and N elemental analyses were carried out with an Elementary Vario El analyzer. IR spectroscopic spectra were performed on a Magna-IR 750 spectrophotometer in the 4000-400 cm^{-1} region on KBr pellets. Variable-temperature magnetic susceptibility measurements were performed on a Quantum Design MPMS SQUID magnetometer. The experimental susceptibilities were corrected for the diamagnetism of the constituent atoms (Pascal's tables).

X-ray data collection and structure refinement.

Single crystals of the six complexes, with suitable dimensions for X-ray diffraction analyses were mounted on glass rods, and the crystal data collected on a Bruker APEXII CCD diffractometer with a Mo Kα sealed tube (λ = 0.71073 Å) using the ω scan mode. For the sake of fully unveiling the HS and LS state, the crystal structure analysis was carried out at 293 K, 100K for **1** and **2**, respectively. The data collection was carried out at 119K for **3**, while that for **4**, **5** and **6** at 293K. The structures were solved using direct methods and expanded using Fourier difference techniques with the SHELXL-2018/3 program package.[34] The non-hydrogen atoms were refined anisotropically with anisotropic displacement coefficients. All the hydrogen atoms were introduced as fixed contributors and assigned isotropic displacement coefficients U(H) =1.2U(C) or 1.5U(C), whose coordinates were allowed to ride on respective carbons using SHELXL-2018/3 and were refined isotropically with fixed U values. The CCDC 2023440-2023447 for complexes **1**-**6**, including the corresponding LS of complexes **1** and **2**, contains the supplementary crystallographic data for this paper and these data can be obtained free of charge from the Cambridge Crystallographic Data Centre via www.ccdc.cam.ac.uk/data_request/cif. Details of the crystal parameters, data collection, and refinement are summarized in Table **S1**(Support Information).

Conflicts of interest

There are no conflicts to declare.

Acknowledgements

This work was supported by the Natural Science Foundation of China (21671121and 21773006) and the Spanish Ministerio de Ciencia e Innovación (MICINN) and FEDER founds (PID2019-106147GB-I00), Unidad de Excelencia María de Maeztu (CEX2019-000919-M).

Supporting Information.

Table S1 contains the selected crystallographic information for compounds **1-6**. Figures S1-S5 show the IR of complexes **1**, **2**, **4**, **5**, **6**. Figure S6 shows the coordination environment of the metal ions (top) and 2D sheet structure along *b* axis for complex **3**. Figure S7 shows the fragment of the $[Fe(3,3'\text{-bipy})]_n^{2+}$ zig-zag chain or $[Fe(3,3'\text{-azpy})]_n^{2+}$ linear chain surrounded by $[Hg(SeCN)_4]^{2-}$ tetrahedrons. Figures S8-S10 shows the magnetic property of complex **4-6**. Figure S11 shows the experimental and simulated SCO behavior of compound **1** and compound **2**.

REFERENCES

(1) Manrique-Juárez, M. D.; Rat, S.; Salmon L.; Molnár, G.; Quintero, C. M.; Nicu, L.; Shepherd H. J.; Bousseksou, A. Switchable molecule-based materials for micro- and nanoscale actuating applications: Achievements and prospects. *Coord. Chem. Rev*. **2016**, *308*, 395–408.

(2) Nihei, M.; Ida, H.; Nibe, T.; Moeljadi, A. M. P.; Trinh, Q. T.; Hirao, H.; Ishizaki, M.; Kurihara, M.; Shiga T.; Oshio, H. Ferrihydrite particle encapsulated within a molecular organic cage. *J. Am. Chem. Soc*. **2018**, *140*, 17753-17759.

(3) Kumar K. S.; and Ruben, M. Sublimable spin crossover complexes: rom spin-state switching to molecular devices. *Angew. Chem. Int. Ed*. **2020**, *59*, 2-22.

(4) König, E. Nature and dynamics of the spin-state interconversion in metal complexes, *Struct. Bond.* **1991**, *76*, 51-152.

(5) Gutlich, P.; Hauser A.; Spiering, H. Thermal and optical switching of iron(II) complexes. *Angew. Chem. Int. Ed*. **1994**, *33*, 2024–2054.

(6) Real, J. A.; Gaspar, A. B.; Niel V.; Muñoz, M. C. Communication between iron(II) building blocks in cooperative spin transition phenomena. *Coord. Chem. Rev*. **2003**, *236*, 121-141.

(7) Nihei, M.; Yanai, Y.; Hsu, I. J.; Sekine Y.; Oshio, H. A hydrogen-bonded cyanide-bridged $[Co_2Fe_2]$ square complex exhibiting a three-step spin transition. *Angew. Chem. Int. Ed*. **2017**, *56*, 591–594.

(8) *Spin crossover in transition metal compounds,* eds. Gütlich P.; and Goodwin, H. A. Springer, Berlin, New York, **2004**.

(9) Real, J. A.; Gaspar, A. B.; Muñoz, M. C. Thermal, pressure and light switchable spin-crossover materials. *Dalton Trans.* **2005**, 2062-2079.

(10) Li, B.; Wang, X. N.; Kirchon, A.; Qin, J. S.; Pang, J. D.; Zhuang, G. L.; Zhou, H. C. Sophisticated Construction of Electronically Labile Materials: A Neutral, Radical-Rich, Cobalt Valence Tautomeric Triangle. *J. Am. Chem. Soc.* **2018**, *140*, 14581-14585.

(11) Li, B.; Zhao, Y. M.; Kirchon, A.; Pang, J. D.; Yang, X. Y.; Zhuang, G. L.; Zhou, H. C. Unconventional Method for Fabricating Valence Tautomeric Materials: Integrating Re-

dox Center within a Metal–Organic Framework. *J. Am. Chem. Soc.* **2019**, *141*, 6822-6826.
(12) *Spin-crossover materials: properties and applications*, eds. Halcrow, M. A. John Wiley & Sons, **2013**.
(13) Nicolazzi W.; Bousseksou, A. Spin crossover phenomenon. *C. R. Chimie.* **2018**, *21*, 1055-1299.
(14) Hofmann K. A.; Höchtlen, F. Abnorme verbindungen des nickels. *Chem. Ber*. **1903**, *36*, 1149-1151.
(15) Hofmann K. A.; Arnoldi, H. Auffällige unterschiede homologer cyclischer moleküle im verhalten gegen nickelcyanürammoniak. *Chem. Ber*. **1906**, *39*, 339-344.
(16) *Inclusion Compounds*, eds. Atwood, J. L.; Davies J. E. D.; MacNicol, D. D. Academic Press, London, **1984**.
(17) *Inclusion Compounds*, eds. Atwood, J. L.; Davies J. E. D; MacNicol, D. D. Oxford University Press, London, UK, **1991**.
(18) Kitazawa, T.; Gomi, Y.; Takahashi, M.; Takeda, M.; Enomoto, M.; Miyazaki A.; Enoki, T. Spin-crossover behaviour of the coordination polymer $Fe^{II}(C_5H_5N)_2Ni^{II}(CN)_4$. *J. Mater. Chem*. **1996**, *6*, 119.
(19) Niel, V.; Martinez-Agudo, J. M.; Muñoz, M. C.; Gaspar A. B.; Real, J. A. Cooperative Spin Crossover Behavior in Cyanide-Bridged Fe(II)−M(II) Bimetallic 3D Hofmann-like Networks (M = Ni, Pd, and Pt). *Inorg. Chem*. **2001**, *40*, 3838.
(20) Niel, V.; Muñoz, M. C.; Gaspar, A. B.; Galet, A.; Levchenko G.; Real, J. A. Thermal-, pressure-, and light-induced spin transition in novel cyanide-bridged Fe^{II}-Ag^{I} bimetallic compounds with three-dimensional interpenetrating double structures $\{Fe^{II}L_x[Ag(CN)_2]_2\}\cdot G$. *Eur. J*. **2002**, *8*, 2446-2453.
(21) Muñoz, M. C.; Real, J. A. Thermo-, piezo-, photo- and chemo-switchable spin crossover iron(II)-metallocyanate based coordination polymers. *Coord. Chem. Rev*. **2011**, *255*, 2068-2093.
(22) Ni, Z.-P.; Liu, J.-L.; Hoque, Md. N.; Liu, W.; Li, J.-Y.; Chen Y.-C.; Tong, M.-L. Recent advances in guest effects on spin-crossover behavior in Hofmann-type metal-organic frameworks. *Coord. Chem. Rev*., **2017**, *335*, 28-43.
(23) Lan, W.-L.; Francisco, J. V. M.; Hao, X.-Y.; Dou, Y.; Muñoz, M. C.; Zhou, Z.; Liu, H.; Liu, Q.-Y.; Real J. A.; Zhang, D.-P. An unprecedented hetero-bimetallic three-dimensional spin crossover coordination polymer based on the tetrahedral $[Hg(SeCN)4]^{2-}$ building block. *Chem. Commun*. **2019**, *55*, 4607–4610.
(24) Trzop, E.; Zhang, D. P.; Piñeiro-Lopez, L.; Valverde-Muñoz, F. J.; Carmen Muñoz, M.; Palatinus, L.; Guerin, L.; Cailleau, H.; Real, J. A.; Collet, E. First step towards a devil's staircase in spin-crossover materials, *Angew. Chem. Int. Ed*., **2016**, *128*, 8817–8821.
(25) Zhang, D.-P.; Trzop, E.; Valverde-Munñoz, F. J.; Piñeiro-López, L.; Muñoz, M. C.; Collet, E.; Real, J. A. Competing phases involving spin-state and ligand structural orderings in a multistable two-dimensional spin crossover coordination polymer. *Crystal Growth & Des*. **2017**, *17*, 2736-2745.
(26) Zhang, D.-P.; Valverde-Munñoz, F. J.; Bartual-Murgui, C.; Piñeiro-López, L.; Muñoz, M. C.; Real, J. A. $\{[Hg(SCN)_3]_2(\mu\text{-}L)\}^{2-}$: An efficient secondary building unit for the synthesis of 2D iron(II) spin-crossover coordination polymers. *Inorg. Chem*. **2018**, *57*, 1562−1571.

(27) Slichter, C. P.; Drickamer, H. G. Pressure-induced electronic changes in compounds of iron, *J. Chem. Phys.* **1972**, *56*, 2142-2160.
(28) Hauser, A. Intersystem crossing in Fe(II) coordination compounds, *Coord. Chem. Rev*. **1991**, *111*, 275-290.
(29) Hauser, A.; Vef, A.; Adler, P. Intersystem crossing dynamics in Fe(II) coordination compounds. *J. Chem. Phys*., **1991**, *95*, 8710-8717.
(30) Hauser, A.; Enachescu, C.; Daku, M. L.; Vargas, A.; Amstutz, N. Low-temperature lifetimes of metastable high-spin states in spin-crossover and in low-spin iron(II) compounds: The rule and exceptions to the rule. *Coord. Chem. Rev*. **2006**, *250*, 1642-1652.
(31) Halcrow, M. A.; Létard, J. F.; Chastanet, G.; Guionneau, P.; Desplanches, C. *Optimizing the stability of trapped metastable spin states in spin-crossove materials: Properties and applications*, eds. John Wiley & Sons Ltd, Oxford, UK, **2013**.
(32) Beadle, P. J.; Goldstein, M.; Goodgame, D. M. L.; Grzeskowiak, R. Metal complexes of azopyridines. II. Complexes of bivalent cobalt, nickel, and copper with 3,3'- and 4,4'-azopyridines. *Inorg. Chem*. **1969**, *8*, 1490–1493.
(33) Adams, C. J.; Haddow, M. F.; Harding, D. J.; Podesta, T. J.; Waddington, R. E. Iron(II) thio- and selenocyanate coordination networks containing 3,3'-bipyridine. *CrystEngComm.* **2011**, *13*, 4909-4914.
(34) Sheldrick, G. M. Crystal structure refinement with SHELXL, *ActaCryst.,* **2015**,*71*, 3-8.
(35) Sorai, M.; Seki, S. Phonon coupled cooperative low-spin $^1A_1$ high-spin $^5T_2$ transition in $[Fe(phen)_2(NCS)_2]$ and $[Fe(phen)_2(NCSe)_2]$ crystals. *J. Phys. Chem. Solids*. **1974**, *35*, 555–570.
(36) Bradley, G.; McKee, V.; Nelson, S. M.; Nelson, J. $^5T_2$-$^1A_1$ Transitions in six-co-ordinate iron(II) complexes of 2,2′-bi-2-thiazoline and 2,2′-bi-4,5-dihydrothiazine ligands. *J. Chem. Soc., Dalton Trans*. **1978**, *5*, 522-526.
(37) König, E.; Ritter, G.; Irler, W.; Nelson, S. M. The high-spin($^5T_2$)⇌low-spin($^1A_1$) transition in solid dithiocyanatobis(2,2'-bi-2,thiazoline)iron(II). Hysteresis effects, debye-waller factors and crystallographic changes. *Inorg. Chim. Acta*. **1979**, *37*, 169-179.
(38) König, E.; Ritter, G.; Dengler, J.; Nelson, J. Detailed study of the quintet. dblharw. singlet spin transition in bis(selenocyanato)bis(2,2'-bi-2-thiazoline) iron (II). *Inorg. Chem*. **1989**, *28*, 611-613.
(39) Moliner, N.; Muñoz, M. C.; Létard, S.; Létard, J. F.; Solans, X.; Burriel, R.; Castro, M.; Kahn, O.; Real, J. A. Spin-crossover in the $[Fe(abpt)_2(NCX)_2]$ (X=S, Se) system: structural, magnetic, calorimetric and photomagnetic studies. *Inorg. Chim. Acta*. **1999**, *291*, 279-288.
(40) Niel, V.; Gaspar, A. B.; Muñoz, M. C.; Abarca, B.; Ballesteros, R.; Real, J. A. Spin Crossover Behavior in the Iron(II)−2-pyridyl [1,2,3] triazolo [1,5-*a*] pyridine System: X-ray Structure, Calorimetric, Magnetic, and Photomagnetic Studies. *Inorg. Chem*. **2003**, *42*, 4782-4788.
(41) Sheu, C.-F.; Chen, K.; Chen, S.-M.; Wen, Y.-S; Lee, G.-H.; Chen, J.-M.; Lee, J.-F.; Cheng, B.-M.; Sheu, H.-S.; Yasuda, N.; Ozawa, Y.; Toriumi, K.; Wang, Y. Structure and Electronic Configuration of an Iron(II) Complex in a LIESST State: A Pump and Probe Method. *Chem. Eur. J*. **2009**, *15*, 2384-2393.
(42) Arcís-Castillo, Z.; Piñeiro-López, L.; Muñoz, M. C.; Ballesteros, R.; Abarca, B.; Real, J. A. Structural, magnetic and calorimetric studies of a crystalline phase of the spin crossover compound $[Fe(tzpy)_2(NCSe)_2]$. *CrystEngComm*. **2013**, *15*, 3455.

(43) Romero-Morcillo, T.; Valverde-Muñoz, F. J.; Piñeiro-López, L.; Carmen Muñoz, M.; Romero, T.; Molina, P.; Real, J. A. Spin crossover in iron(II) complexes with ferrocene-bearing triazole-pyridine ligands. *Dalton Trans*. **2015**, *44*, 18911-18918.
(44) Bartual-Murgui, C.; Piñeiro-López, L.; Valverde-Muñoz, F. J.; Muñoz, M. C.; Seredyuk, M.; Real, J. A. Chiral and Racemic Spin Crossover Polymorphs in a Family of Mononuclear Iron(II) Compounds. *Inorg. Chem*. **2017**, *56*, 13535-13546.
(45) Neville, S. M.; Leita, B. A.; Offermann, D. A.; Duriska, M. B.; Moubaraki, B.; Chapman, K. W.; Halder, G. J.; Murray, K. S. Spin-Crossover Studies on a Series of 1D Chain and Dinuclear Iron(II) Triazine-Dipyridylamine Compounds. *Eur. J. Inorg. Chem*. **2007**, *8*, 1073-1085.
(46) Ross, T. M.; Moubaraki, B.; Turner, D. R.; Halder, G. J.; Chastanet, G.; Neville, S. M.; Cashion, J. D.; Létard, J.-F.; Batten, S. R.; Murray, K. S. Spin crossover and solvate effects in 1D Fe^{II} chain compounds containing bis(dipyridylamine)-linked triazine ligands. *Eur. J. Inorg. Chem*. **2011**, *9*, 395–1417.
(47) Neville, S. M.; Leita, B. A.; Halder, G. J.; Kepert, C. J.; Moubaraki, B.; Létard, J. F.; Murray K. S. Understanding the Two-Step Spin-Transition Phenomenon in Iron(II) 1D Chain Materials. *Chem.-Eur. J*. **2008**, *14*, 10123-10133.
(48) Vreugdenhil, W.; Van Diemen, J. H.; De Graaff, R. A. G.; Haasnoot, J. G.; Reedijk, J.; Van Der Kraan, A. M.; Kahn, O.; Zarembowitch, J. High-spin α low-spin transition in $[Fe(NCS)_2(4,4'\text{-bis-}1,2,4\text{-triazole})_2](H_2O)$. X-ray crystal structure and magnetic, mössbauer and EPR properties. *Polyhedron*, **1990**, *9*, 2971-2979.
(49) Vreugdenhil, W.; Haasnoot, J. G.; Kahn, O.; Thuéry, P.; Reedijk, J. A copper(II) dope as a detector for the high-spin .tautm. low-spin transition in the two-dimensional compound [trans-bis(thiocyanato)bis(4,4'-bi-1,2,4-triazole) iron] hydrate. *J. Am. Chem. Soc*., **1987**, *109*, 5272–5273.
(50) Ozarowski, A.; Shunzhong, Y.; McGarvey, B. R.; Mislankar, A.; Drake, J. E. EPR and NMR study of the spin-crossover transition in bis(4,4'-bi-1,2,4-triazole) bis(thiocyanato)iron hydrate and bis(4,4'-bi-1,2,4-triazole) bis(selenocyanato)iron hydrate. X-ray structure determination of $Fe(4,4'\text{-bi-}1,2,4\text{-triazole})_2(SeCN)_2$.cntdot.$H_2O$. *Inorg. Chem*. **1991**, *30*, 3167-3174.
(51) Adams, C. J.; Muñoz, M. C.; Waddington, R. E.; Real, J. A. Cooperative Spin Transition in the Two-Dimensional Coordination Polymer $[Fe(4,4'\text{-bipyridine})_2(NCX)_2]\cdot 4CHCl_3$ (X = S, Se). *Inorg. Chem*. **2011**, *50*, 10633-10642.
(52) Adams, C. J.; Haddow, M. F.; Harding, D. J.; Podesta, T. J.; Waddington, R. E. Iron(ii) thio- and selenocyanate coordination networks containing 3,3'-bipyridine. *CrystEngComm*, **2011**, *13*, 4909-4914.

Graphical abstract:

Spin crossover in a series of non-Hofmann type Fe(II) coordination polymers based on $[Hg(SeCN)_3]^-$ or $[Hg(SeCN)_4]^{2-}$ building blocks

We report a series of 2D and 3D 6,4-connected hetero-bimetallic Hg^{II}-Fe^{II} coordination polymers derived from self-assembling Fe^{II}, $[Hg(SeCN)_4]^{2-}$ and bis-monodentate pyridine-like linkers (L). The results show how sensitive the topological structure is with respect to the coordination ability, flexibility structural conformation of the bridging ligand (L) and how it determines the occurrence or not of spin crossover behavior in de series.